Materials Research Express

PAPER

Elastic properties of single crystal $Bi_{12}SiO_{20}$ as a function of pressure and temperature and acoustic attenuation effects in $Bi_{12}MO_{20}$ (M = Si, Ge and Ti)

Eiken Haussühl[1], **Hans Josef Reichmann**[2], **Jürgen Schreuer**[3], **Alexandra Friedrich**[1,4], **Christian Hirschle**[3], **Lkhamsuren Bayarjargal**[1], **Björn Winkler**[1], **Igor Alencar**[5], **Leonore Wiehl**[1,6] and **Steffen Ganschow**[7]

[1] Institut für Geowissenschaften, Goethe-Universität Frankfurt, Altenhöferallee 1, D-60438 Frankfurt a.M., Germany
[2] Helmholtz-Zentrum Potsdam, Deutsches Geoforschungszentrum—GFZ, Telegrafenberg, D-14473 Potsdam, Germany
[3] Institut für Geologie, Mineralogie und Geophysik, Ruhr-Universität Bochum, Universitätsstrasse 150, D-44801 Bochum, Germany
[4] Present Address: Institut für Anorganische Chemie, Julius-Maximilians-Universität Würzburg, Am Hubland, D-97074 Würzburg, Germany
[5] Instituto de Física, Universidade Federal do Rio Grande do Sul, Avenida Bento Gonçalves 9500, CEP-91501-970 Porto Alegre-RS, Brazil
[6] Present Address: Technische Universität Darmstadt, Otto-Berndt-Strasse 3, D-64287 Darmstadt, Germany
[7] Leibniz-Institut für Kristallzüchtung (IKZ), Max-Born-Strasse 2, D-12489 Berlin, Germany

E-mail: haussuehl@kristall.uni-frankfurt.de

Keywords: sillenites, elasticity, piezoelectricity, ultrasound damping, resonant ultrasound spectroscopy, Brillouin spectroscopy, high pressure and temperature

OPEN ACCESS

RECEIVED
3 November 2019

REVISED
3 January 2020

ACCEPTED FOR PUBLICATION
13 January 2020

PUBLISHED
4 February 2020

Abstract

A comprehensive study of sillenite $Bi_{12}SiO_{20}$ single-crystal properties, including elastic stiffness and piezoelectric coefficients, dielectric permittivity, thermal expansion and molar heat capacity, is presented. Brillouin-interferometry measurements (up to 27 GPa), which were performed at high pressures for the first time, and *ab initio* calculations based on density functional theory (up to 50 GPa) show the stability of the sillenite structure in the investigated pressure range, in agreement with previous studies. Elastic stiffness coefficients c_{11} and c_{12} are found to increase continuously with pressure while c_{44} increases slightly for lower pressures and remains nearly constant above 15 GPa. Heat-capacity measurements were performed with a quasi-adiabatic calorimeter employing the relaxation method between 2 K and 395 K. No phase transition could be observed in this temperature interval. Standard molar entropy, enthalpy change and Debye temperature are extracted from the data. The results are found to be roughly half of the previous values reported in the literature. The discrepancy is attributed to the overestimation of the Debye temperature which was extracted from high-temperature data. Additionally, Debye temperatures obtained from mean sound velocities derived by Voigt-Reuss averaging are in agreement with our heat-capacity results. Finally, a complete set of electromechanical coefficients was deduced from the application of resonant ultrasound spectroscopy between 103 K and 733 K. No discontinuities in the temperature dependence of the coefficients are observed. High-temperature (up to 1100 K) resonant ultrasound spectra recorded for $Bi_{12}MO_{20}$ crystals revealed strong and reversible acoustic dissipation effects at 870 K, 960 K and 550 K for M = Si, Ge and Ti, respectively. Resonances with small contributions from the elastic shear stiffness c_{44} and the piezoelectric stress coefficient e_{123} are almost unaffected by this dissipation.

1. Introduction

The cubic mineral sillenite, $Bi_{12}SiO_{20}$, first found at Durango, Mexico (Frondel 1943), is closely related to γ-Bi_2O_3 synthesized by Sillen in 1938 (Sillen 1938). γ-Bi_2O_3 is metastable at ambient conditions (Wells 1984), but can be stabilized by addition of metal oxides leading to the general sillenite composition $Bi_{12}M_xO_{20\pm\delta}$. In stoichiometric sillenites M is tetravalent and the oxygen lattice is fully occupied ($x = 1, \delta = 0$) (Wiehl *et al* 2010). The most

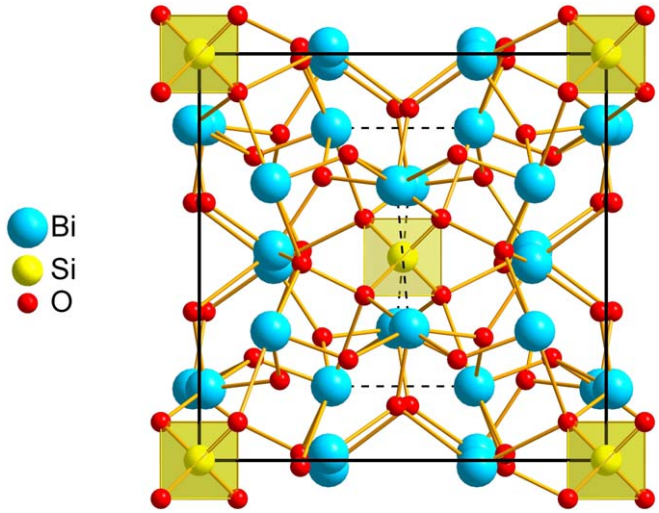

Figure 1. Crystal structure of BSO at ambient conditions (Wiehl *et al* 2010). The Bi^{3+} $6s^2$ lone electron pairs are oriented along the closest Bi-Bi contacts which are plotted as dashed lines.

prominent members of the sillenite family are those with M = Si, Ge, and Ti, which are abbreviated in the following as BSO, BGO, and BTO (Tissot and Lartigue 1988, Yu and Min 2004, Wiehl *et al* 2010, Melńikova *et al* 2011, Wiehl *et al* 2013).

The sillenite structure type (space group $I23$) is characterized by MO_4 tetrahedra located at the center and the corners of the cubic unit cell. These tetrahedra are linked by $BiO_5\square$ octahedra where the stereochemically active Bi^{3+} $6s^2$ lone electron pair partially fills the unoccupied site $\square$ (figure 1). In combination with the lack of inversion symmetry this is the source of outstanding electrical and optical properties suitable for photorefractive applications (Buse 1997, Baade *et al* 2001, Georges *et al* 2001). For example, sillenites are used in devices utilized for optical computing, optical information processing, and high-sensitive photo detectors (Tempel 1993, Filippov *et al* 2000). Sillenite single crystals exhibit low acoustic wave velocities and are therefore candidates for delay lines in electronic circuits (Melńikova *et al* 2011). Due to its high photosensitivity BSO can be used as light moduator as well as a crystal for recording and reproducing phase holograms (Melńikova *et al* 2011).

Electromechanical coupling effects allow the conversion of mechanical into electrical energy and vice versa. The fundamental properties for this type of conversion are the elasticity, piezoelectricity and permittivity. Sillenites exhibit large piezoelectric effects, i.e. d_{123} of BSO is about 20 pC N^{-1}, which is about 8 times larger than d_{111} of α-Quartz, and they are potential piezoelectric materials for electromechanical applications (Shen *et al* 2014).

In contrast to their high potential for applications, surprisingly little is known about the elastic behavior of sillenites at non-ambient conditions especially at high pressures above tens of GPa and high temperatures close to their melting points. Full sets of elastic stiffness coefficients have been reported for BSO in the temperature range of 250 K–300 K (Gospodinov *et al* 1988, 1992) and at pressures up to 0.16 GPa (Gospodinov *et al* 1988). Shen *et al* (2014) investigated full sets of electromechanical parameters of BSO and BTO between 300 K and 773 K. The stability of BSO up to 770 K was confirmed by Raman-spectroscopic measurements (Salke and Rao 2012).

Recently, the pressure-dependence of the structures of BTO, BSO and BGO have been studied up to 37 GPa, 39 GPa and 50 GPa, respectively, and the vibrational properties of BSO up to 39 GPa, (Rao *et al* 2010, Wiehl *et al* 2010, 2013). Broadening of X-ray reflections and anomalies of the BSO and BTO lattice compression in comparison to the behavior of related sesquioxides were attributed to a high sensitivity of the sillenite structure to even slight deviatoric stress rather than to the occurrence of a phase transition.

Considering the potential scientific and industrial importance of sillenites and in order to complement our earlier work on sillenites, we report here on the complete sets of elastic stiffness coefficients, c_{ij}, of BSO, determined by resonant ultrasound spectroscopy (RUS) in the temperature range from 103 K to 733 K, Brillouin interferometry up to 27 GPa and by density functional theory (DFT) based model calculations in the athermal limit. The DFT calculations were carried out in order to extrapolate the c_{ij} coefficients beyond the experimental pressure limits. RUS experiments up to 1123 K were performed on BSO, BGO and BTO to study the temperature dependence of ultrasound dissipation effects in sillenites.

Finally, standard molar entropy, enthalpy change and Debye temperature were extracted from low-temperature heat capacity measurements. Heat capacity measurements of BSO were performed only at elevated temperatures so far (Suleimenova and Skorikov 1992, Licea and Ioanid 1999, Denisova *et al* 2010,

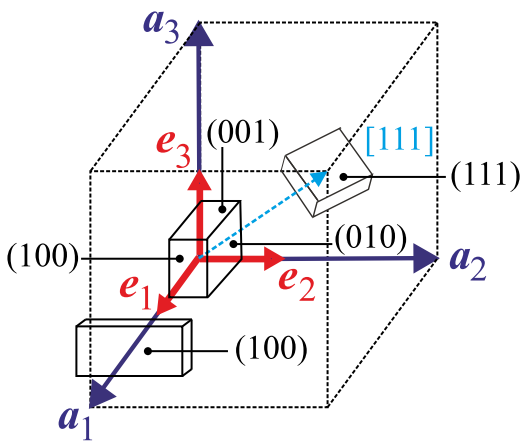

Figure 2. Rectangular parallelepiped (main cut) used for RUS experiments and two additional oriented crystal cuts (100) and (111) in respect to a crystallographic ($\boldsymbol{a}_i$) and Cartesian crystal-physical reference system ($\boldsymbol{e}_i$). Dotted lines represent the cubic unit cell and the arrow with the dashed line points to the crystallographic direction [111].

Table 1. Lattice parameter a_1 taken from literature (Wiehl *et al* 2010, 2013), dimensions l_i of RUS-samples and densities ρ_{xray} (derived from unit cell volume and ideal chemical composition), ρ_b (determined by buoyancy method in pure water at 293 K) and ρ_G (calculated from dimensions and mass of RUS-samples) of investigated sillenite samples at ambient conditions.

Compound	Sample no.	a_1 Å	l_1 mm	l_2 mm	l_3 mm	ρ_{xray} g cm^{-3}	ρ_b g cm^{-3}	ρ_G g cm^{-3}
BSO	BSO-1a	10.105(1)	6.308(2)	4.732(2)	4.355(2)	9.19(1)	9.207(5)	9.16(1)
BSO	BSO-3	10.105(1)	5.257(2)	6.202(2)	7.970(2)	9.19(1)	9.203(5)	9.17(1)
BGO	BGO-3	10.147(1)	5.887(2)	7.218(2)	8.020(2)	9.22(1)	9.249(5)	9.20(1)
BTO	BTO-1	10.181(1)	5.547(2)	7.084(2)	8.021(2)	9.05(1)	9.086(5)	9.01(1)

Onderka 2015) and some discrepancies were observed in the previously published data. Hence, here we perfomed measurements between 2 K and 395 K.

2. Experimental details

2.1. Sample preparation

All BSO and BGO samples used in this investigation were grown by the Czochralski technique, BTO was grown by the top-seeded flux method. A slightly reddish brown single crystal of BSO with about 10 mm in diameter and 20 mm in length was purchased from Vladimir L. Tarasov (Russia). Samples from the same boule were used in our recent high-pressure synchrotron diffraction study (Wiehl *et al* 2010). Electron microprobe analyses revealed an almost pure stoichiometric composition. Two further BSO single crystals were provided by the IKZ, Germany, for dielectric permittivity measurements. BGO was provided by Daniel S. Pantsurkin (Nikolaev Institute of Inorganic Chemistry, Russia). Samples of BTO were purchased from the Sillenites Ltd. company (Russia). Lattice parameters and densities as derived from X-ray diffraction experiments are summarized in table 1.

The physical properties reported here are referred to a Cartesian reference system with basis vectors $\boldsymbol{e}_i$, which are connected to the crystallographic basis vectors $\boldsymbol{a}_i$ of the cubic unit cell according to $\boldsymbol{e}_i \parallel \boldsymbol{a}_i$.

For Brillouin scattering experiments platelet samples were cut from the BSO raw crystal and polished on two parallel sides. Their orientations were controlled by X-ray diffraction. Scattering experiments at ambient conditions were carried out on platelets with dimensions of about 0.2 mm × 1 mm × 1 mm and plate-normals parallel to [100] (edge of the cubic unit cell) and [111] (space diagonal of the cubic unit cell), respectively (figure 2). For studies at high pressures using a diamond anvil cell platelets with plate-normals parallel to [100] and dimensions of about 0.01 mm × 0.06 mm × 0.06 mm were employed.

For RUS experiments rectangular parallelepipeds with edges parallel to $\boldsymbol{e}_i$ and edge lengths l_i of about 5 mm to 8 mm (table 1) were cut from large single crystals using a low-speed diamond saw and were polished on glass plates using a mixture of water and Al_2O_3 powder (grain size between 5 μm and 12 μm). In the case of BGO the sample was additionally polished to optical quality. The sample orientation was controlled by X-ray diffraction.

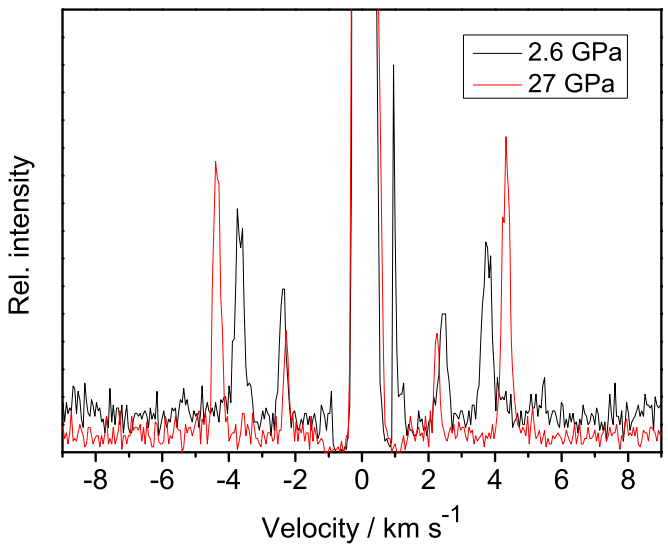

Figure 3. Examples of Brillouin spectra of BSO at pressures of 2.6 GPa and 27 GPa.

The deviation from ideal orientation was kept below 0.4° and the deviation from plane-parallelism of opposing faces was smaller than ±2 μm.

For the measurements of the dielectric permittivity of BSO thin plates of about 1 mm thickness and diameters ranging from 12 mm to 15 mm were cut parallel to the crystallographic faces (100) and (111). The samples were polished flat with a deviation from plane parallelism of ±2 μm. The large faces were covered with silver electrodes.

2.2. Brillouin scattering

For high-pressure experiments the BSO samples were loaded in a Boehler-Almax diamond anvil cell (Boehler 2006). The culets of the diamonds were 300 μm in diameter; the gasket material was tungsten, or rhenium for pressures >14 GPa. The gaskets with an initial thickness of 200 μm were pre-indented to thicknesses between 31 μm and 47 μm for the high-pressure runs. Holes of 140 μm to 170 μm in diameter were machined in the gaskets by means of a laser lathe. In all high-pressure runs helium was used as the pressure-transmitting medium in order to guarantee that the non-hydrostaticity was as low as possible (Wiehl *et al* 2013). Pressures were determined using the ruby R1 fluorescence-shift calibration according to Mao *et al* (1986). A vertically polarized solid state laser (λ_0 = 532 nm, output during experiments = 700 mW) and a 6-pass-tandem Fabry–Perot interferometer by JRS Scientific Instruments were employed for the Brillouin experiments. All measurements were performed in forward symmetric geometry. The details of this technique have been described elsewhere (Sinogeikin *et al* 1998, Speziale and Duffy 2002, Sinogeikin *et al* 2004). In brief, the incoming laser beam is scattered by thermally activated acoustic phonons in the sample and analyzed and detected by the Brillouin-interferometer using a photo multiplier tube. The scattering angle θ (the angle between incident and scattered beam) was 60°. At each pressure, 12 Brillouin spectra were collected at χ-angles between 0° and 180° (examples are depicted in figure 3).

In forward geometry, the Brillouin frequency shift $\Delta\omega$ is related to the acoustic velocity v through

$$v = \frac{\Delta\omega\lambda_0}{2\sin(\theta/2)} \tag{1}$$

where λ_0 is the laser wavelength and θ is the scattering angle. Using the platelet geometry, the refractive index of the sample cancels out (Whitfield *et al* 1976). The single crystal elastic coefficients have been calculated from the acoustic velocities $v_{P,S}$ of the longitudinal pressure (P) and shear waves (S) by a least-squares inversion of the Christoffel's equation (Every 1979, 1980).

2.3. Resonant ultrasound spectroscopy, dilatometry and dielectric permittivity measurements

The thermoelastic and the piezoelectric behavior of BSO as well as the ultrasound dissipation of BSO, BGO and BTO were studied with resonant ultrasound spectroscopy (RUS) (Leisure and Willis 1997, Migliori and Sarrao 1997). For this purpose a custom-built high-temperature RUS-device was employed (Haussühl *et al* 2011, 2012). The temperature stability inside the furnace (1600 °C furnace type 6.219.1–26 from Netzsch) achieved by a cascading temperature controller (EPC 900 from Eurotherm) was better than ±0.5 K. The

accuracy of the S-type thermocouple at the maximum temperature was better than ±10 K. For the temperature dependent RUS measurements the samples were slightly clamped at opposite corners between the ends of two horizontally arranged corundum ceramic rods which acted simultaneously as ultrasonic wave guides. The ultrasound generator and detector were mounted on the cold ends of the corundum rods outside the heated area. The force acting on the opposed corners of the sample was kept below 0.05 N. This ensured that the experimental setup fulfilled the conditions of a nearly freely vibrating body. In the case of the high-temperature RUS measurements which were performed in air the signal generation and detection was achieved using network analyzers (HP4194A and 4394A from Keysight) in combination with a high speed signal amplifier (type 4400 and HSA4101 from NF-electronics). In addition, low-temperature RUS measurements were performed in a He atmosphere on a second BSO sample in a commercial resistance furnace (500 °C furnace type 6.219.1–22 from Netzsch). Signal generation and detection was achieved using a network analyzer and a signal amplifier (FRA5087 and BA4825 from NF Corporation) also employing two corundum ceramic rods as in the case for high-temperature measurements. Temperature measurement and control involved the furnace, liquid nitrogen cooling, type E thermocouples and a cascading temperature controller (2704 from Eurotherm).

Resonance spectra in the frequency range between 50 kHz and 800 kHz with a resolution of 0.0025 kHz were collected between 293 K and 1073 K in steps of 10 K for BSO and BTO, respectively, and between 293 K and 1123 K in steps of 5 K for BGO. For a second sample of BSO further RUS-measurements were conducted from ambient conditions down to 103 K in steps of 20 K and up to 713 K in steps of 10 K. Temperature stability was within ±0.1 K. The frequency range for the low-temperature measurements was 100 kHz to 1250 kHz with a resolution of 0.01 kHz. At each temperature step the samples were first allowed to equilibrate for at least 30 minutes before the resonance spectrum was recorded.

In order to study the effects of accoustic dissipation the profiles of selected resonances were approximated by modified Lorentzians according to

$$A_i(f) = A_{0i}\left(1 + \frac{(f - f_i)^2}{0.25 \cdot \mathrm{w}_i^2}\right)^{n_i} \tag{2}$$

where A_{0i} and f_i are amplitude and frequency, respectively, of the specific ith eigenmode. The exponent n_i describes the shape of the resonance peak which also affects its value of the full-width at half-maximum (fwhm). w_i corresponds to the fwhm Δf_i which is related to the inverse quality factor Q_i^{-1} of the resonance by

$$Q_i^{-1} = \frac{\Delta f_i}{f_i}. \tag{3}$$

In the case of BSO the independent elastic coefficients c_{11}, c_{12} and c_{44}, and the piezoelectric stress coefficient e_{123} were derived for each temperature from the corresponding resonance spectrum using the frequencies of at least 100 observed eigenmodes. The evaluation was carried out by a non-linear least-squares procedure in which the observed resonance frequencies were compared to those calculated from sample dimensions, experimental density, dielectric permittivity and a trial set of elastic coefficients and piezoelectric stress coefficient. Initial values of c_{ij} were taken from literature (Schweppe and Quadflieg 1974, Gospodinov *et al* 1988, Yu and Min 2004, Shen *et al* 2014). The calculated resonance frequencies were obtained by solving a general eigenvalue problem, the rank of which was equivalent to the number of basis functions used for the development of the components of the displacement vector. In the non-linear least-squares refinement procedure the quantity

$$\chi^2 = \sum_{i=1}^{n} w_i \cdot (\omega_i^2(\mathrm{calc}) - \omega_i^2(\mathrm{obs})^2 \tag{4}$$

calculated for n circular eigenmodes with resonance frequencies $f_i = \omega_i/2\pi$ was minimized by varying the elastic coefficients c_{ij}^E at constant electric field and the piezoelectric stress coefficient e_{123} of the sample. The w_i are individual weights calculated by assuming experimental errors of ±0.1 kHz for each observed resonance frequency. In order to minimize errors due to truncation effects, up to 8775 normalized Legendre polynomials were used for the expansion of the displacement vector. The code for the RUS-refinement also provides the means for checking the influence of each refined coefficient in a given mode.

Dielectric permittivity measurements were performed at 295 K applying the geometric method to thin plane-parallel plates with arbitrary shape and a network analyzer (HP 4194 from Keysight) in a frequency range between 10 kHz and 10 MHz. For the calculation of the relative dielectric permittivity at constant stress the following equation was applied

$$\epsilon_{11}^{\sigma} / \epsilon_0 = \frac{t^2 \rho C_{\mathrm{el}}}{M \epsilon_0} \tag{5}$$

where t is the thickness, ρ the density, C_{el} the capacity and M the mass of the sample, respectively. ϵ_0 denotes the permittivity of vacuum. The change of the relative dielectric permittivity at constant stress within the

temperature range between 300 K and 700 K was neglected due to a minor variation in $\epsilon_{11}^{\sigma}/\epsilon_0$ of about ±1% (Shen *et al* 2014).

The accurate determination of the temperature dependence of the elastic coefficients requires also a correction for changes in sample dimensions and density due to thermal expansion effects (Haussühl *et al* 2012). In order to determine the independent coefficient of thermal expansion of BSO, the temperature-induced strain was studied between 100 K and 1070 K on plane-parallel plates using two commercial inductive gauge dilatometers (DIL 402C from Netzsch) equipped with a low-temperature or a high-temperature furnace, respectively. The BSO-sample was measured at least three times with heating/cooling rates of 1 K min^{-1} under He purge gas atmosphere for the low-temperature dilatometer and air for the high-temperature dilatometer. The dilatometers were calibrated with standard samples made of fused silica or α-Al_2O_3.

2.4. Heat capacity measurements

The heat capacity measurements were performed at temperatures between 2 K and 395 K using a relaxation calorimeter (heat capacity option of the Physical Properties Measurement System (PPMS) from Quantum Design). A single crystal with a mass of 35.57(2) mg was measured at 150 different temperatures from 395 K to 2 K with logarithmically-reduced steps. At each temperature, the heat capacity was measured three times by the relaxation method using the two-τ model (Kennedy *et al* 2007). The samples were thermally coupled to the sapphire holder by Apiezon N grease. The absolute accuracy of our experiments was checked by measuring the standard reference materials SRM-720 (Al_2O_3) and Cu (Alfa Aesar, 99.999%). The deviation of our data for SRM-720 from those published by Ditmars *et al* (1982) was within 2% in the range of 395 K to 50 K and within 6% below 5 K. The deviation of our data for Cu from those reported by Lashley *et al* (2003) was 1% in the range from 300 K to 40 K, and 2% below 40 K.

Molar heat capacities were fitted with polynomials of higher order to facilitate the numerical integration. The standard molar entropy $S^{\circ}_{298.15}$ and the enthalpy change between 0 K and 298.15 K, $\triangle H_{0-298.15}$, were computed with the following equations:

$$S^{\circ}_{298.15} = \int_0^{298.15} \frac{C_p}{T} dT \tag{6}$$

and

$$\triangle H_{0-298.15} = \int_0^{298.15} C_p dT. \tag{7}$$

Neglecting the difference between C_p and C_V at lower temperatures, the Debye temperature Θ_{Cp} can be determined using

$$C_V = \frac{12\pi^4}{5} nR \left(\frac{T}{\Theta_{Cp}} \right)^3 \tag{8}$$

where n is the number of atoms per unit cell and $R = 8.314\,46$ J mol^{-1} K^{-1} (Carslaw and Jaeger 1959).

2.5. Computational details

DFT-based calculations were performed with academic and commercial versions of the CASTEP program (Milman *et al* 2000, Clark *et al* 2005, CASTEP User Guide 2008) using a generalized gradient approximation in the Wu-Cohen formulation (Wu and Cohen 2006). For all calculations, ultrasoft pseudopotentials from the CASTEP data base were generated 'on the fly', with 6, 5 and 4 valence electrons for O, Bi and Si, respectively. The maximum cutoff energy of the plane waves was 800 eV. In addition to the cutoff energy, the quality of the calculations was determined by the density of the grid of k-points in the Brillouin zone. Here, distances between the points were less than 0.036 $Å^{-1}$. The wave vectors for the sampling points were chosen according to the scheme proposed by Monkhorst and Pack (1976). Full geometry optimization calculations were performed. Structures were considered to be converged when the largest residual component of the stress tensor was less than 0.02 GPa and the largest residual force acting on an atom was less than 0.01 eV $Å^{-1}$. The elastic stiffness coefficients were obtained as the proportionality constants between applied strains and resultant stresses. Strain patterns were imposed with several magnitudes up to a maximum strain amplitude of 0.003, and after geometry optimization of the internal parameters the resultant stresses were computed. The present calculations are restricted to the athermal limit, in which temperature effects and zero-point motions were neglected. The calculations of the elastic stiffness coefficients were performed for 5 pressure points between 0 GPa and 50 GPa.

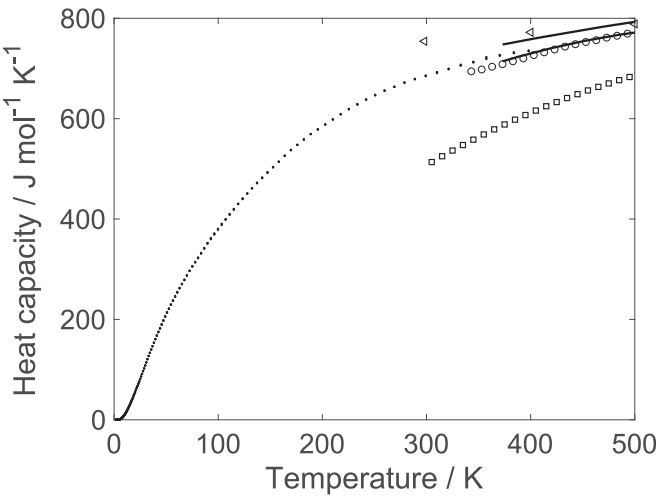

Figure 4. The molar heat capacity C_p of BSO measured between 2 K and 395 K. Our experimental data are shown as dots. Lines, triangles, circles and squares represent the results by Suleimenova and Skorikov (1992), Denisova *et al* (2010), Onderka (2015), and Licea and Ioanid (1999), respectively.

3. Results and discussion

3.1. Heat capacity measurements

Previous heat capacity measurements of BSO were performed only at elevated temperatures using DSC or DTA so far (Suleimenova and Skorikov 1992, Licea and Ioanid 1999, Denisova *et al* 2010, Onderka 2015). Figure 4 shows the heat capacity data obtained here together with the results of previous studies. Our heat capacities around 400 K are in good agreement with the results by Onderka (2015) and one of the measurements by Suleimenova and Skorikov (1992). However, these data are 3% smaller than our results at around 350 K. The other measurement by Suleimenova and Skorikov (1992) and the data by Denisova *et al* (2010) differ up to 5% from our measurement. The results by Licea and Ioanid (1999) differ significantly by about 15% from our and other previous studies. We assume that the reason for this large deviation might be a reduced thermal contact of the polycrystalline samples to the sample holder. No phase transition was observed between 395 K and 2 K using heat capacity measurements.

The enthalpy of BSO at 298.15 K is 131.8(13) kJ mol^{-1} and the standard entropy computed from the heat capacities using equation (6) is 926(9) J K^{-1} mol^{-1}. The Debye temperature derived from our heat capacity measurements is $\Theta_{\mathrm{Cp}} = 248(2)$ K (figure 5). Onderka (2015) estimated the standard entropy of BSO using an extrapolation of the low-temperature heat capacity data from his high-temperature heat capacities applying the Debye model. This led to an overestimation of the Debye temperature ($\Theta_{\mathrm{Cp}} = 686(13)$ K) , which further resulted in an underestimated value of 517(72) J K^{-1} mol^{-1} for the standard entropy in his study. It differs by more than 40% from our results.

3.2. Elastic properties at ambient conditions

The single-crystal elastic stiffness coefficients and aggregate moduli of BSO are compared with those reported by various authors in table 2. The elastic coefficients obtained at ambient conditions by RUS and Brillouin spectroscopy in this study and by Gospodinov *et al* (1988) (improved Schaefer-Bergmann method) are in excellent agreement within experimental errors (table 2). The c_{ij} values of our theoretical study using DFT-calculations valid for ambient pressure and 0 K are in reasonable agreement with the experimental data, while being systematically larger. The results by Yu and Min (2004) (Brillouin interferometry) as well as Schweppe and Quadflieg (1974) are comparable with our results (table 2). The single-crystal elastic stiffness coefficients c_{11} and c_{12} by Shen *et al* (2014) deviate considerably from the results of this paper (table 2).

The elastic stiffness coefficients can be used to estimate mean sound velocities which then can be employed to compute the Debye temperature according to Robie and Edwards (1966)

$$\Theta_{\mathrm{elastic}} = (h/k)[(3nN\rho)/(4\pi M)]^{1/3} v_m, \tag{9}$$

where h and k are the Planck and Boltzmann constants, n is the number of atoms per formula unit, N is Avogadro's number, M the formula weight and v_m the mean sound velocity, respectively. A rough estimation of the mean sound velocity v_m was computed according to the approach described by Robie and Edwards (1966)

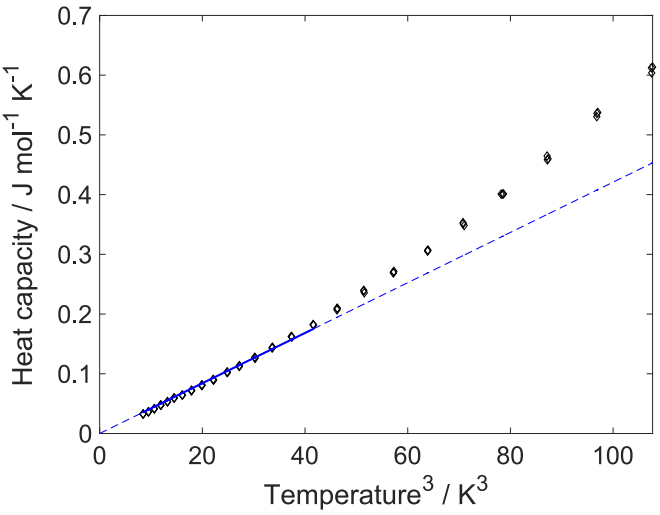

Figure 5. Linear fit of the molar heat capacity of BSO for the determination of the Debye temperature based on equation (8). Black symbols are the measured data; the blue line is the fitted function. Error bars are smaller than the symbol size.

Table 2. Experimental elastic and electrical properties of BSO at ambient conditions and calculated elastic properties for 0 K. ρ density, $\epsilon^{\sigma}_{11}/\epsilon_0$ relative dielectric permittivity at constant stress, $\epsilon^{x}_{11}/\epsilon_0$ relative dielectric permittivity at constant strain, e_{123} piezoelectric stress coefficient, d_{123} piezoelectric strain coefficient. Method of determination of elastic stiffnesses: RUS^E (resonant ultrasound spectroscopy), BS (Brillouin spectroscopy), DFT (density functional theory), RAR^E (resonance-antiresonance technique), PR^E (plate-resonance technique, improved Schaefer-Bergmann method) and PE^E (pulse-echo technique), E measurements at constant electric field (c^E_{ij}). K_{0s} adiabatic bulk modulus. g deviation from Cauchy relations, c^{iso}_{ii} aggregate elastic coefficients (average of Voigt and Reuss model).

Reference	this work				(Shen *et al* 2014)	(Yu and Min 2004)	(Gospodinov *et al* 1988)	(Schweppe and Quadflieg 1974)
Sample no.	BSO-1a	BSO-3	—	—	—	—	—	—
ρ/g cm^{-3}	9.207(5)	9.203(5)	—	—	9.2	9.2	9.197	9.21
$\epsilon^{\sigma}_{11}/\epsilon_0$	42.6 (5)	42.6 (5)	—	—	48.2	—	—	47
$\epsilon^{x}_{11}/\epsilon_0$	39.7(5)	39.7(5)	—	—	—	—	36	42
Method	RUS^E	RUS^E	BS	DFT	RAR^E	BS	PR^E	PE^E
c_{11} / GPa	131.2(4)	130.2(1)	129(2)	146(4)	119	134.3	129.8	128
c_{12} / GPa	30.3(4)	29.6(1)	30(2)	41(2)	43	30.6	29.71	28
c_{44} / GPa	24.67(2)	24.64(1)	25(1)	34(4)	25	26.4	24.72	25
e_{123} / C m^{-2}	1.16(4)	1.11(1)	—	—	1.2	—	0.8	1.0
d_{123} / pC N^{-1}	23.6(7)	22.5(2)	—	—	24	—	16	20
K_{0s} / GPa	63.9(5)	63.1(5)	63(1)	76(5)	68.3	65.2	63.08	61.3
$g = c_{12}$–c_{44} / GPa	5.6(6)	5.0(2)	5(1)	7(2)	18	4.2	5.0	3
c^{iso}_{11} / GPa	107.9(6)	107.1(2)	107(4)	130(5)	107.8	111.5	107.0	105.5
c^{iso}_{44} / GPa	33.0(4)	33.0(4)	33(2)	41(6)	29.6	34.7	32.9	33.1

$$v_m = [1/3((1/v_l^3) + (2/v_s^3))]^{-1/3}, \tag{10}$$

where v_l and v_s are the longitudinal and shear sound velocities, respectively, using the aggregate (isotropic) elastic values c^{iso}_{11} and c^{iso}_{44} (table 2) derived by the Voigt-Reuss averaging. This calculation yielded $\Theta_{\mathrm{elastic}} = 251$ K which is in reasonable agreement with $\Theta_{\mathrm{Cp}} = 248(2)$ K derived from our heat capacity measurements (figure 5) and with $\Theta_{\mathrm{elastic}} = 238$ K reported by Licea and Ioanid (1999).

The extracted piezoelectric coefficient e_{123} of our work is compatible with the data from literature (table 2).

3.3. Temperature dependence of strain and elastic and piezoelectric properties

Temperature-dependent measurements reveal strong ultrasound dissipation at elevated temperatures (figure 6), thus reliable c_{ij} coefficients could only be obtained up to 733 K. Between 103 K and 773 K the evolution of the c_{ij} (figure 7) and e_{123} (figure 8), respectively, with temperature is almost linear. The small deviations between the two linear fitting curves of e_{123} might stem from sample preparation of BSO-1a and from different internal sample quality. However, the temperature dependent coefficients $\partial e_{123}/\partial T$ are similar within experimental uncertainties. Results of corresponding fits are presented in table 3. A comparison with the results of

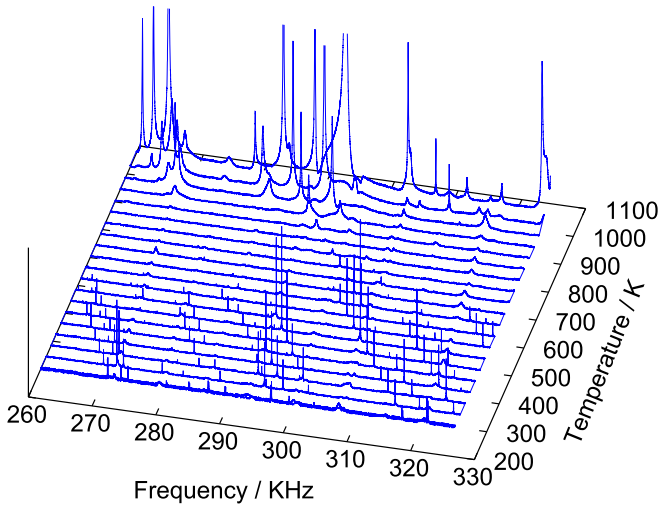

Figure 6. Selected region of the resonant ultrasound spectra for BSO single crystal (no. 3) as a function of temperature.

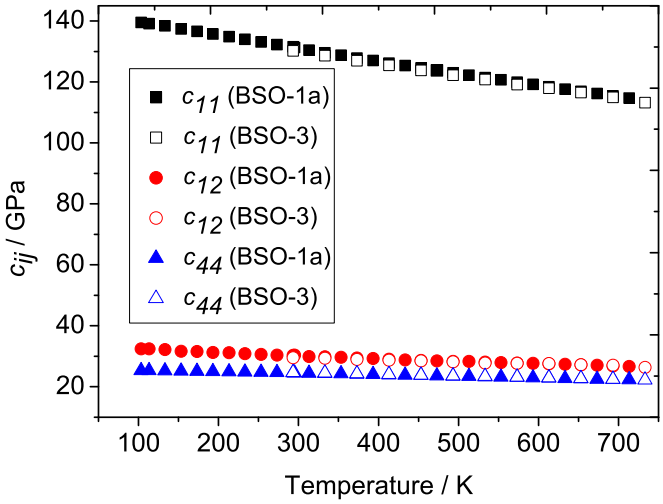

Figure 7. Single-crystal elastic stiffness coefficients c_{ij} of BSO as a function of temperature. Experimental errors are within the size of the symbols.

Gospodinov *et al* (1988) reveals reasonable agreement of the temperature coefficients for c_{11} and c_{44} but a discrepancy of about 40% in the case of c_{12}.

The thermal expansion of BSO is slightly non-linear (figure 9), thus second-order polynomials of the type

$$x_{ij}(T) = \alpha_{11}\Delta T + \beta_{11}(\Delta T)^2 \tag{11}$$

with $\Delta T = T - T_0$ are required for a proper approximation of the strains x_{ij} over the entire investigated temperature range. $T_0 = 293$ K denotes the reference temperature and $\alpha_{11} = 14.4(4) \cdot 10^{-6}\,\mathrm{K}^{-1}$, and $\beta_{11} = 2.8(1) \cdot 10^{-9}\,\mathrm{K}^{-2}$ are the corresponding coefficients of linear and quadratic thermal expansion, respectively. Our linear thermal expansion coefficient deviates from the reported value of Gospodinov *et al* (1988) by about 20%.

3.4. Acoustic attenuation of BSO, BGO and BTO

The sound attenuation encouraged us to investigate additionally the quality factors of selected resonances of BSO and related BGO and BTO up to 1123 K. We observed strong and reversible acoustic dissipation effects, which are characterized by Debye peak-like attenuation maxima at about 870 K for BSO, at 960 K for BGO and at 550 K for BTO, respectively (figure 10). Debye peaks are typical for anelastic relaxation processes of point defects (Nowick and Berry 1972). Modes with small contributions of the elastic shear stiffness c_{44} and of the piezoelectric stress coefficient e_{123} are almost unaffected by the dissipation (see e.g. mode no. 21 of BGO-3, figure 11). The nearly linear evolution of frequency with temperature for this mode is depicted in figure 11(a),

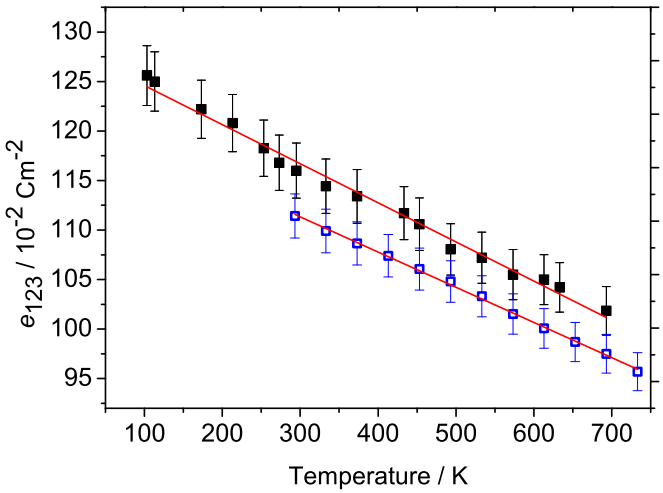

Figure 8. Evolution of the piezoelectric stress coefficient e_{123} of BSO as a function of temperature. Filled black symbols denote sample no. 1a, open blue symbols sample no. 3, respectively. Red lines represent linear fitting curves.

Table 3. Experimental thermoelastic properties of BSO at ambient pressure as derived by linear regressions with reference temperature $T_0 = 295$ K from experimental data. The evolution of c_{44} with temperature was fitted using the polynominal regression of the type $c_{ij}(T) = c_{ij}^0 + c_{ij}^1(T - T_0) + c_{ij}^2(T - T_0)^2$. Numbers in parentheses are the uncertainties of the last digit as derived from the standard deviations of the corresponding fit parameters. The thermoelastic coefficients $T_{ij} = \partial \log c_{ij}/\partial T$ are for 295 K. Method of determination of elastic stiffnesses: RUS (resonant ultrasound spectroscopy), PR (plate resonance technique, improved Schaefer-Bergmann method).

Reference	this work		(Gospodinov *et al* 1988)
Method	RUS		PR
Sample no.	BSO-1a	BSO-3	
Temperature range/K	103–713	293–733	250–320
T_{11} / 10^{-3} K^{-1}	−0.313(2)	−0.316(3)	−0.297(8)
T_{12} / 10^{-3} K^{-1}	−0.303(7)	−0.304(7)	−0.439(20)
T_{44} / 10^{-3} K^{-1}	−0.195(2)	−0.191(2)	−0.182(6)
$\partial c_{11}/\partial T$ / MPa K^{-1}	−41.1(2)	−41.1(4)	−38.6(10)
$\partial c_{12}/\partial T$ / MPa K^{-1}	−9.2(2)	−9.0(2)	−13.0(6)
$\partial c_{44}/\partial T$ / MPa K^{-1}	−4.79(4)	−4.7(1)	−4.5(2)
$\partial c_{44}^2/\partial T$ / kPa K^{-2}	−1.6(1)	−1.8(3)	—
$\partial e_{123}/\partial T$ / 10^{-2}C m^{-2} K^{-1}	−0.039(2)	−0.036(1)	—

whereas a strong peak of the inverse quality factor could be detected at about 960 K (figure 11(b)). Therefore, piezoelectric/carrier relaxation as observed for example in piezoelectric langasite type materials (Johnson *et al* 2008, Fritze 2010, Hirschle and Schreuer 2018) might play an important role here, too. A more detailed study of the frequency dependence of the dissipation maxima would allow for the determination of activation energies offering a deeper insight into the underlying atomistic processes.

3.5. Pressure dependence of elastic properties

To the best of our knowledge, besides the low-pressure data up to 0.16 GPa (Gospodinov *et al* 1988), no high-pressure data of single-crystal elastic stiffness coefficients c_{ij} has been reported so far. Brillouin measurements were performed up to 27 GPa. No indications for pressure-induced amorphisation or structural phase transition were observed. In figure 12, the three independent single-crystal elastic stiffness coefficients are depicted as a function of

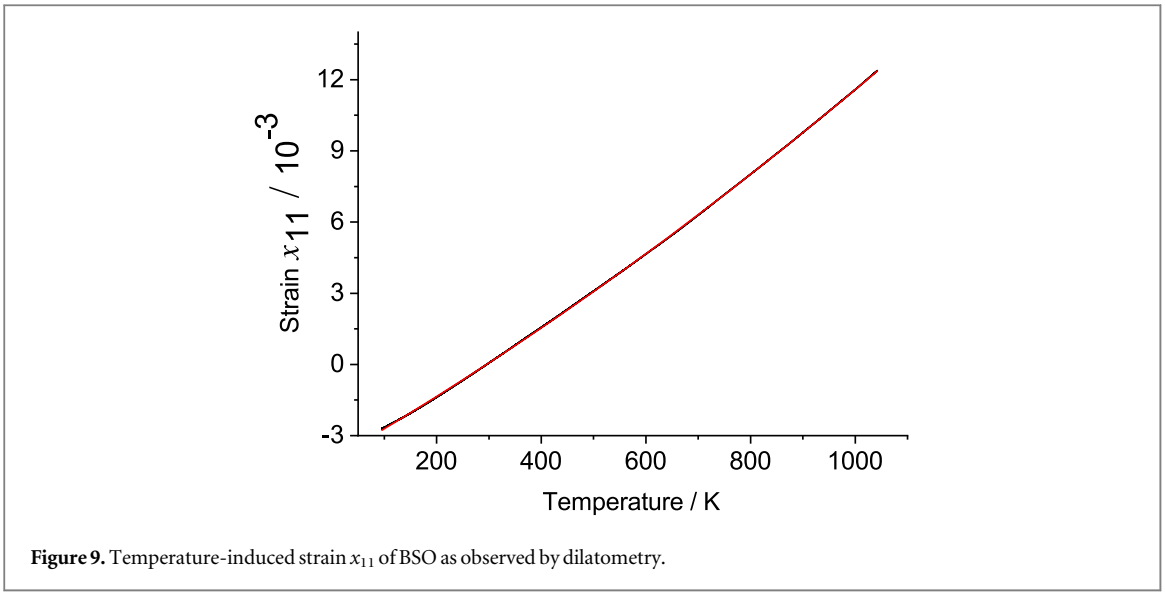

Figure 9. Temperature-induced strain x_{11} of BSO as observed by dilatometry.

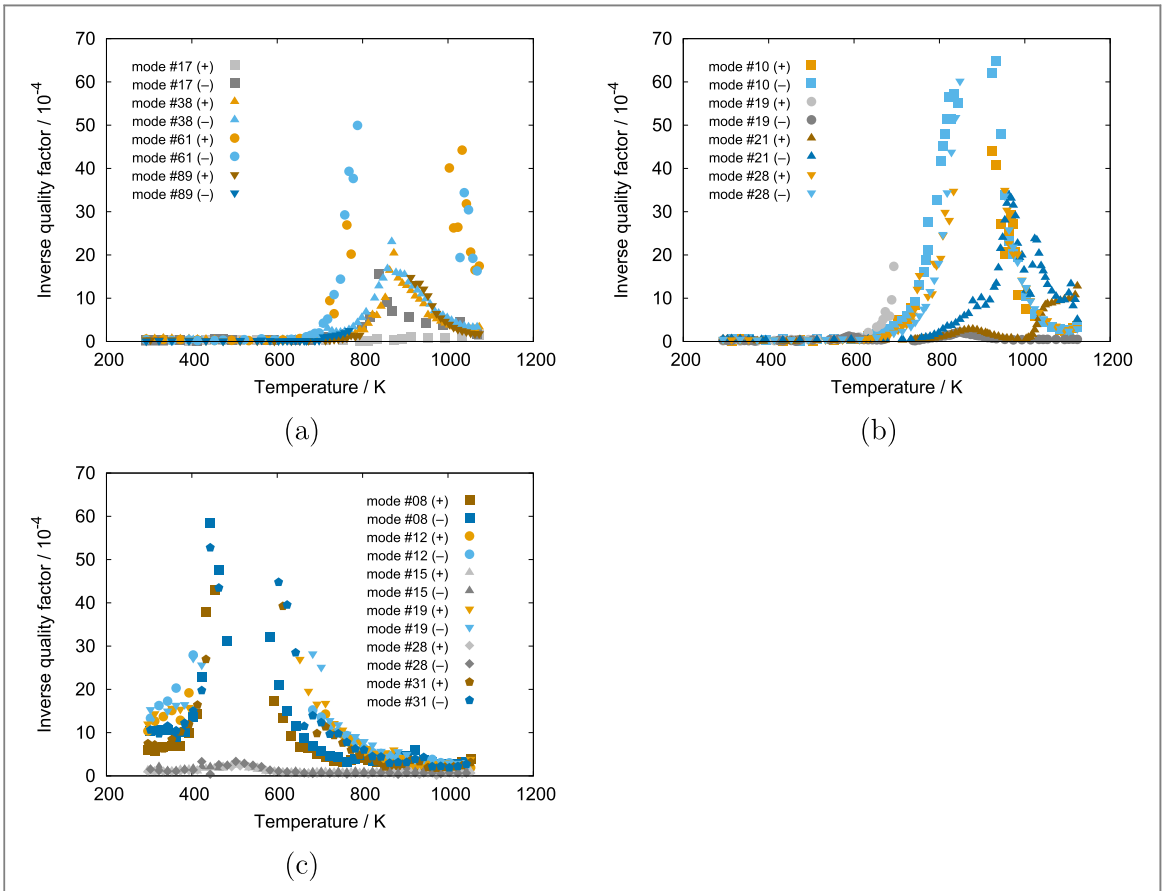

Figure 10. Evolution of the inverse quality factor of distinct RUS-modes for (a) BSO, (b) BGO and (c) BTO with temperature. The symbols (+) denote measurements using heating ramps and (-) measurements using cooling ramps, respectively.

pressure up to 27 GPa together with the RUS data at ambient conditions and DFT data calculated up to 50 GPa. The c_{ij} values at ambient conditions by Yu and Min (2004), and Landolt-Börnstein (Landolt and Börnstein 1961) are also shown in figure 12. The first and second pressure derivatives of the elastic stiffness behaviour as well as the adiabatic bulk and shear moduli calculated from the single-crystal moduli (Voigt-Reuss average) of BSO are listed in table 4. The deviations between the low-pressure derivatives dc_{ij}/dp measured by Gospodinov *et al* (1988) and our findings range between 16% and 31% (table 4). The pressure dependencies of the aggregate moduli are depicted in figure 13.

The elastic coefficients c_{11} and c_{12} measured by Brillouin interferometry increase with increasing pressure while c_{44} first increases up to a pressure of 15 GPa and then remains almost constant on further pressure increase to 27 GPa

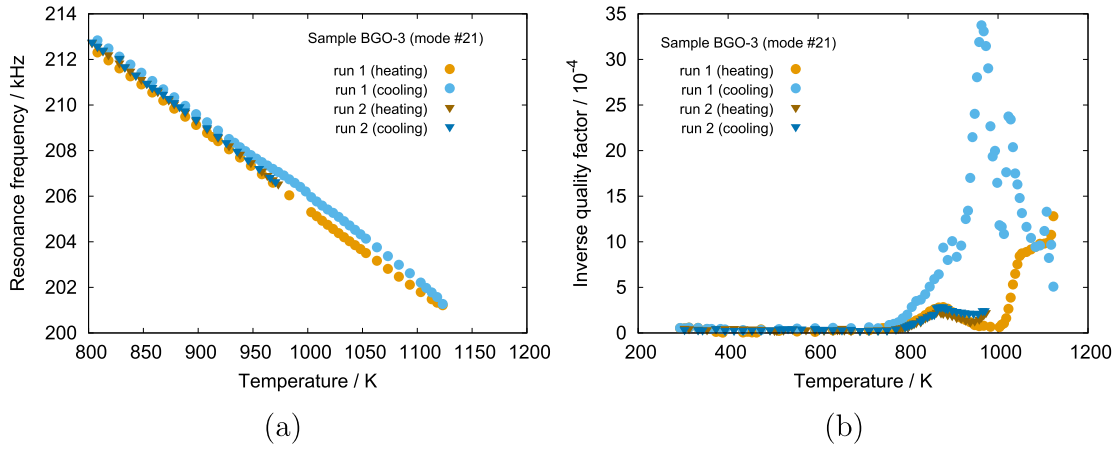

Figure 11. Temperature dependence of (a) frequency and (b) inverse quality factor for mode no. 21 of BGO.

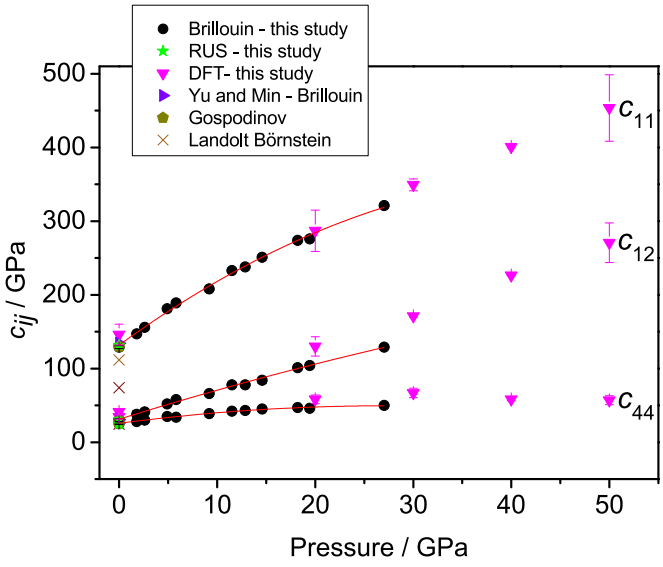

Figure 12. Single-crystal elastic stiffness coefficients c_{ij} of BSO as a function of pressure. The c_{ij} values obtained by means of DFT-calculations show the same trend with pressure as the present experimental study.

(figure 12). At high pressures the curve characteristics of the calculated c_{ij} using DFT are similar to the experimental ones: the elastic stiffness coefficients c_{11} and c_{12} increase while c_{44} flattens with pressure, or may even slightly decrease as can be deduced from the theoretical value at 50 GPa. Both, the non-linear curvatures of the pressure dependencies of c_{11} and c_{44} and the linearity of the c_{12} pressure dependence are well reproduced in experiment and theory. While the absolute agreement of the experimental and theoretical pressure dependencies of elastic tensor components c_{11} and c_{44} is very good, the pressure increase of c_{12} is significantly overestimated in the calculations.

Neither our experimental data nor our theoretical calculations on BSO show any signs of a phase transition in the investigated pressure range up to 27 and 50 GPa, respectively, which is in agreement with the experimental powder X-ray compression data by Rao *et al* (2010) collected up to 26 GPa. Both, the Brillouin as well as the ultrasound measurements (table 2) of this study and the X-ray compression measurements by Wiehl *et al* (2010) result in the same value of the adiabatic and isothermal bulk modulus, namely $K = 63$ GPa (table 4). The relation between adiabatic and isothermal bulk moduli, K_s and K_t, is given by

$$K_s/K_t = (1 + \alpha\gamma_{th}T), \tag{12}$$

where α is the thermal expansion, γ_{th} is the thermodynamic Grüneisen parameter and T is the temperature. The pressure derivative of the adiabatic bulk modulus $K'_{0s} = 6.1(2)$ is also equivalent within uncertainty to the pressure derivative of the isothermal bulk modulus $K'_{0t} = 5.6(5)$ and $K'_{0t} = 6.6(3)$ reported for powder and single crystal X-ray diffraction data, respectively, by Wiehl *et al* (2010, 2013) (table 4). These values are considerably smaller than $K'_{0t} = 16.7$ (with $K_{0t} = 36$ GPa) reported by Rao *et al* (2010) obtained by X-ray

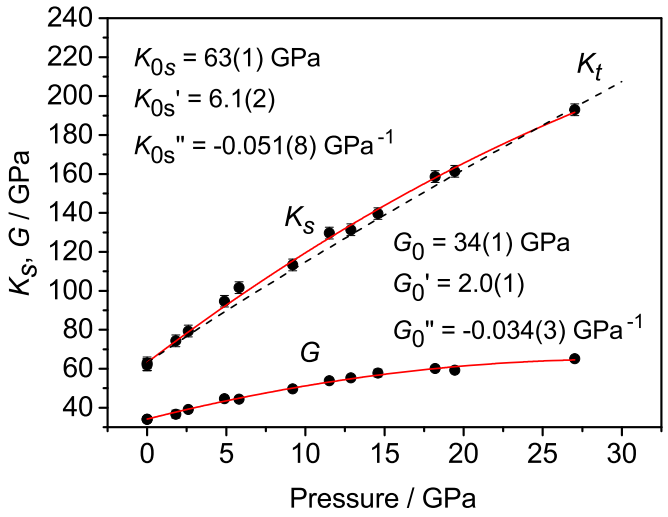

Figure 13. The aggregate bulk and shear moduli (K_s, G) of BSO as a function of pressure. The dashed black line indicates the isothermal bulk modulus K_t determined by Wiehl *et al* (2010).

Table 4. Pressure derivatives of elastic stiffness of BSO for room temperature from this study (2nd order polynomial fit) and from literature. K_{0s} adiabatic bulk (GPa) and G_0 shear moduli (GPa) calculated from the c_{ij} coefficients (Voigt - Reuss average), K_{0t} isothermal bulk modulus (GPa).

Reference	This work	(Gospodinov *et al* 1988)	(Wiehl *et al* 2010)	(Rao *et al* 2010)
p_{max}/GPa	27	0.16	23	24
$c'_{11} = P_{11}$	9.7(4)	11.55(2)	—	—
c''_{11} / GPa^{-1}	−0.10(2)	—	—	—
$c'_{12} = P_{12}$	4.2(3)	5.7(3)	—	—
c''_{12} / GPa^{-1}	−0.02(1)	—	—	—
$c'_{44} = P_{44}$	1.7(1)	2.48(8)	—	—
c''_{44} / GPa^{-1}	−0.029(4)	—	—	—
K_{0s} / GPa	63(1)	63.08	—	—
K_{0t} / GPa	—	—	63(4)	36
K'_{0s}	6.1(2)	—	—	
K'_{0t}	—	—	5.6(5)	16.7
K''_{0s} / GPa^{-1}	−0.051(8)	—	—	—
G_0 / GPa	34(1)	—	—	—
G'_0	2.0(1)	—	—	—
G''_0 / GPa^{-1}	−0.034(3)	—	—	—

compression measurements on powder samples up to 24 GPa (table 4). This inconsistency in both the bulk modulus and its pressure derivative reported by Rao *et al* (2010) if compared to the other existing data, might be partly attributed to the use of an alcohol mixture as the pressure-transmitting medium, which is known to provide hydrostatic conditions only below 10 GPa (Klotz *et al* 2009).

Rao *et al* (2010) determined the mode Grüneisen parameters from Raman measurements on BSO. These values lie in a small range $0.14 < \gamma_i < 0.84$ (Rao *et al* 2010). To estimate the thermodynamic Grüneisen parameter γ_{th}, the average of the mode Grüneisen parameters is taken, $\langle\gamma_i\rangle = \gamma_{th} = 0.38$. Given the fact, that the thermal expansion α_{11} of BSO is between $14.4{\cdot}10^{-6}$ K^{-1} and $16{\cdot}10^{-6}$ K^{-1} (this work and Salke and Rao (Salke and Rao 2012)) the isothermal bulk modulus K_{0t} is calculated to be 63.1 GPa, which fits within experimental error to the experimental results of K_{0s} of this work and K_{0t} by Wiehl *et al* (2010).

The anisotropy according to the definition by Zener (1947) $A = 2c_{44}/(c_{11}-c_{12})$ and the ratio of the maximum and minimum of the longitudinal elastic stiffness $c'(\mathbf{u}) = u_i u_j u_k u_l c_{ijkl}$ with pressure of BSO is shown in figure 14, where u_i are the direction cosines. The anisotropy increases slightly from 0.5 at ambient pressure to 0.54 at 10 GPa and decreases subsequently to 0.52 at highest pressure of this study. The fact that the anisotropy of BSO does not change drastically with pressure supports the findings by Wiehl *et al* (2013) that the crystal structure is stable up to 39 GPa.

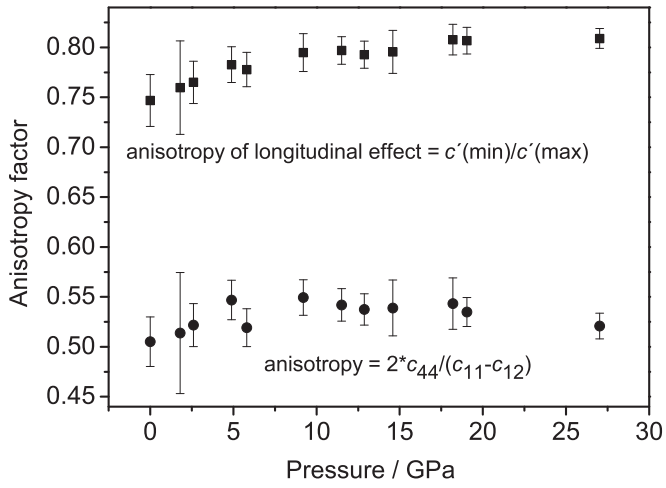

Figure 14. Anisotropy factor $A = 2c_{44}/(c_{11}-c_{12})$ and ratio of minimum and maximum longitudinal elastic stiffness, $c'(\mathrm{min})/c'(\mathrm{max})$ versus pressure of BSO.

3.6. Conclusions

The cubic crystal structure of BSO exhibits a remarkable pressure stability despite its high compressibility. Single-crystal Brillouin measurements up to 27 GPa and *ab initio* calculations by density functional theory up to 50 GPa show no indications of a structural phase transition in this pressure range. We found that the elasticity coefficients c_{11} and c_{12} continuously increase with pressure while c_{44} only slightly increases and remains nearly constant within standard deviation above 15 GPa. In addition, the elastic properties of sillenites were investigated with the aid of resonant ultrasound spectroscopy (RUS) between 100 K and ca. 1100 K. We observed surprisingly strong and reversible acoustic dissipation effects, which are characterized by attenuation peaks at about 870 K for BSO, at 960 K for BGO, and at 550 K for BTO, respectively. Those peaks resemble Snoek-effect like anelastic relaxation peaks (Nowick and Berry 1972). However, modes with small contributions of the elastic shear stiffness c_{44} and also small piezoelectric stress coefficient e_{123} are almost unaffected by the dissipation. Therefore, piezoelectric/carrier relaxation, which was also observed in piezoelectric langasite type materials (Johnson *et al* 2008, Fritze 2010, Hirschle and Schreuer 2018), might play an important role here as well. A more detailed study of the frequency dependence of the dissipation maxima would allow for the determination of activation energies offering a deeper insight into the underlying atomistic processes.

Acknowledgments

The authors gratefully acknowledge Danil S. Pantsurkin (Nikolaev Insitute of Inorganic Chemistry SB RAS, Novosibirsk, Russia) for the provision of BGO crystals and the Deutsche Forschungsgemeinschaft, DFG for financial support of this investigation (HA 5137/3 and HA 5137/5). AF appreciates financial support from the DFG within priority program SPP-1236 (FR 2491/2–1).

ORCID iDs

Eiken Haussühl https://orcid.org/0000-0002-3244-8163
Jürgen Schreuer https://orcid.org/0000-0002-8611-6842
Alexandra Friedrich https://orcid.org/0000-0002-1411-7336
Christian Hirschle https://orcid.org/0000-0002-0086-5026
Igor Alencar https://orcid.org/0000-0002-7384-0110
Steffen Ganschow https://orcid.org/0000-0003-1328-1617

References

Baade T, Kiessling A and Kowarschik R 2001 *J. Opt.* **3** 250–4
Boehler R 2006 *Rev. Sci. Instrum.* **77** 115103
Buse K 1997 *Appl. Phys.* B **64** 391–407
Carslaw H and Jaeger J 1959 *Heat in Solids* vol 1 (Oxford: Clarendon)
CASTEP User Guide 2008(San Diego, CA: Accelrys Inc.)

Clark S, Segall M, Pickard C, Hasnip P, Probert M, Refson K and Payne M 2005 *Z. Kristallogr.* **220** 567–70
Denisova L, Irtyugo L, Denisov V and Bironi V 2010 *J. Siberian Fed. Univ. Eng. Technol.* **3** 214–9
Ditmars D, Ishihara S, Chang S, Bernstein G and West E 1982 *J. Res. Natl. Bur. Stand.* **87** 159–63
Every A 1979 *Phys. Rev. Lett.* **42** 1065–8
Every A 1980 *Phys. Rev.* B **22** 1746–60
Filippov V N, Starodumov A N, Barmenkov Y O and Makarov V V 2000 *Appl. Opt.* **39** 1389–93
Fritze H 2010 *J. Electroceram.* **26** 122–61
Frondel C 1943 *Acta Cryst.* **28** 521–35
Georges M P, Scauflaire V S and Lemaire P C 2001 *Appl. Phys.* B **72** 761–5
Gospodinov M, Haussühl S, Sveshtarov P, Dobreva S and Sampil A 1992 *Mat. Res. Bull.* **27** 1415–21
Gospodinov M, Haussühl S, Sveshtarov P, Tassev V and Petkov N 1988 *Bulg. J. Phys.* **15** 140–3
Haussühl E, Schreuer J, Winkler B, Haussühl S, Bayarjargal L and Milman V 2012 *J. Phys.: Condens. Matter* **24** 345402
Haussühl E, Vinograd V L, Krenzel T F, Schreuer J, Wilson D J and Ottinger J 2011 *Z. Kristallogr.* **226** 236–53
Hirschle C and Schreuer J 2018 *IEEE Trans. Ultrason. Ferroelect. Freq. Control.* **65** 1250
Johnson W L, Schulz M and Fritze H 2008 *IEEE Trans. Ultrason. Ferroelect. Freq. Control.* **61** 1433–41
Kennedy C A, Stancescu M, Marriott R A and White M A 2007 *Cryogenics* **47** 107–12
Klotz S, Chervin J C, Munsch P and Le Marchand G 2009 *J. Phys.* D **42** 075413
Landolt H H and Börnstein R 1961 *Pergamon (Oxford), Course of Theoretical Physics* **4** 495
Lashley J *et al* 2003 *Cryogenics* **43** 369–78
Leisure R and Willis F 1997 *J. Phys.: Condens. Matter* **9** 6001–29
Licea I and Ioanid A 1999 *Phys. Stat. Sol. (b)* **212** 27–36
Mao H, Xu J and Bell P 1986 *J. Geophys. Res.* **91** 4673–6
Melńikova T, Kuzm´icheva G, Rybakov V, Bolotina N and Dubovsky A 2011 *Inorg. Chem.* **50** 2002–9
Migliori A and Sarrao J 1997 *Resonant Ultrasound Spectroscopy* (New York: Wiley)
Milman V, Winkler B, White J, Pickard C, Payne M, Akhmatskaya E and Nobes R 2000 *Int. J. Quantum Chem.* **77** 895–910
Monkhorst H and Pack J 1976 *Phys. Rev.* B **13** 5188–92
Nowick A and Berry B 1972 *Anelastic Relaxation in Crystalline Solids* (New York: Academic)
Onderka B 2015 *Thermochim. Acta* **601** 68–74
Rao R, Garg A and Sakuntala T 2010 *J. Appl. Phys.* **108** 082508
Robie R A and Edwards J L 1966 *J. Appl. Phys.* **37** 2659–63
Salke N and Rao R 2012 *AIP Conf. Proc.* 1447 813–4
Schweppe H and Quadflieg P 1974 *IEEE Trans. Sonics Ultras.* **SU-21** 56–7
Shen C, Zhang H, Zhang Y, Xu H, Yu H, Wang J and Zhang S 2014 *Crystals* **4** 141–51
Sillen L 1938 *Ark. Kemi. Min. Geol.* **12** 1–15
Sinogeikin S, Katsura T and Bass J 1998 *J. Geophys. Res.* **103** 20819–25
Sinogeikin S, Lakshtanov D, Nicholas J and Bass J 2004 *Phys. Earth Planet. Inter.* **143** 575–86
Speziale S and Duffy T 2002 *Phys. Chem. Miner.* **29** 465–72
Suleimenova G S and Skorikov V M 1992 *Thermochim. Acta* **196** 203–11
Tempel C M M v 1993 *Appl. Opt.* **32** 4869–74
Tissot P and Lartigue H 1988 *Thermochim. Acta* **127** 377–83
Wells A 1984 *Structural Inorganic Chemistry* 5th edn (Oxford: Clarendon)
Whitfield C H, Brody E M and Bassett W A 1976 *Rev. Sci. Instrum.* **47** 942–7
Wiehl L, Friedrich A, Haussühl E, Morgenroth W, Biehler J, Winkler B and Hanfland M 2013 *J. Solid State Chem.* **208** 35–42
Wiehl L, Friedrich A, Haussühl E, Morgenroth W, Grzechnik A, Friese K, Winkler B, Refson K and Milman V 2010 *J. Phys.: Condens. Mattter* **22** 505401
Wu Z and Cohen R E 2006 *Phys. Rev.* B **73** 235116
Yu Y and Min B 2004 *J. Eur. Ceram. Soc.* **24** 1161–4
Zener C 1947 *Phys. Rev.* **71** 846–51